ISSN: 2476-6909; Modares. Mech. Eng. *2025;25(05):295-306.*

Modares Mechanical Engineering

DOI: 10.48311/MME.25.5.295
journal homepage: mme.modares.ac.ir

Combined WENO Schemes for Increasing the Accuracy of the Numerical Solution of Conservation Laws

Hossein Mahmoodi Darian*

School of Engineering Science, College of Engineering, University of Tehran, Tehran, Iran

ARTICLE INFO

Article Type
Original Research

Article History
Received: May 02, 2025
Revised: July 14, 2025
Accepted: July 20, 2025
ePublished: August 12, 2025

ABSTRACT

In this article, we introduce a new method which allows utilizing all the available sub-stencils of a WENO scheme to increase the accuracy of the numerical solution of conservation laws while preserving the non-oscillatory property of the scheme. In this method, near a discontinuity, if there is a smooth sub-stencil with higher-order of accuracy, it is used in the reconstruction procedure. Furthermore, in smooth regions, all the sub-stencils of the same order of accuracy form the stencil with the highest order of accuracy as the conventional WENO scheme. The presented method is assessed using several test cases of the linear wave equation and one- and two-dimensional Euler's equations of gas dynamics. In addition to the original weights of WENO schemes, the WENO-Z approach is used. The results show that the new method increases the accuracy of the results while properly maintaining the ENO property.

Keywords: WENO Schemes, Shock-Capturing Schemes, Nonlinear Weights

How to cite this article
Mahmoodi Darian H, Combined WENO schemes for increasing the accuracy of the numerical solution of conservation laws. Modares Mechanical Engineering; *2025;25(05):295-306.*

**Corresponding author's email: hmahmoodi@ut.ac.ir*
**Corresponding ORCID ID: 0000-0002-6063-3235*

1- Introduction

Numerical solution of hyperbolic systems of conservation laws due to the presence of shocks and other discontinuities is a difficult task, especially when using high-order accurate schemes. Among various shock-capturing schemes, Weighted Essentially Non-Oscillatory (WENO) schemes are very popular. They were first introduced in [1,2] and their success led to their use in other shock-capturing schemes. For instance, Bozorgpoor et al. [3] utilized WENO schemes as a nonlinear filter where the flux was discretized using a high-order compact scheme. Also, WENO schemes are an important part of discontinuous Galerkin schemes [4]. Gradually different modifications and improvements over the original WENO schemes [2] were proposed in the literature. Henrik et al. [3] showed that near the critical points, the original weights are not close enough to their optimal values and cannot achieve the maximum accuracy. They introduced mapped WENO schemes (WENO-M), where they used a mapping function for the weights of [2] to recover the maximum order in the critical points. This work made a basis for introducing new mapping functions [6-10] which improved for efficiency in [11-15]. Another improvement was the WENO-Z scheme, which was introduced by Borges et al. [16] which generalized by Castro et al. [17] and further improved in [18-22]. In contrast to [5] and its similar work, they defined new weights, instead of mapping the original weights of [2]. Recently, Amat et al. in a series of papers [23-27] introduced a new WENO interpolation capable of raising the order of accuracy close to discontinuities for some applications such as data interpolation and signal processing. Their idea was to use the highest-order stencil as long as the stencil does not contain any discontinuity. They used their new WENO algorithm for the numerical solution of conservation laws in [28].

In this manuscript, we introduce a general method for using all the available stencils of different orders to increase the accuracy of WENO schemes while preserving the non-oscillatory property of the scheme. The idea is to first compute the flux using a weighted combination of all the sub-stencils of the same order of accuracy and then combine the resulted fluxes to form the final flux. We denote this scheme as combined WENO scheme (WENO-C).

The manuscript is organized as follows. In Section 2, we give a brief description of the WENO schemes. The main part of this work will be presented in Section 3, where we introduce a general formula for combining different stencils of different orders. In Section 4, the new scheme is assessed by numerical simulation of the linear advection equation and Euler equations of gas dynamics. Finally, the concluding remarks are given in Section 5.

2- WENO schemes

In this section, we describe the WENO schemes for discretizing the governing equation of a conservation law. Consider the following equation:

$$u_t + f_x = 0 \tag{1}$$

where u is the conservative variable and $f = f(u)$ is the flux function. We consider a uniform grid in the x-direction and define the grid points as $x_i = i\Delta x$ where Δx is the grid size. The flux derivative is discretized in the conservative form as

$$f'(x_i) = \frac{f_{i+\frac{1}{2}} - f_{i-\frac{1}{2}}}{\Delta x} + O(\Delta x^m) \tag{2}$$

where $f_{i+\frac{1}{2}}$ is the numerical flux at $x_{i+\frac{1}{2}}$ and m is the order of the truncation error. In a $(2k-1)$ th-order WENO scheme [1,2], the flux $f_{i+\frac{1}{2}}$ is approximated such that $m = 2k-1$ in smooth regions and $m = k$ near discontinuities. This is done by a convex combination of k fluxes:

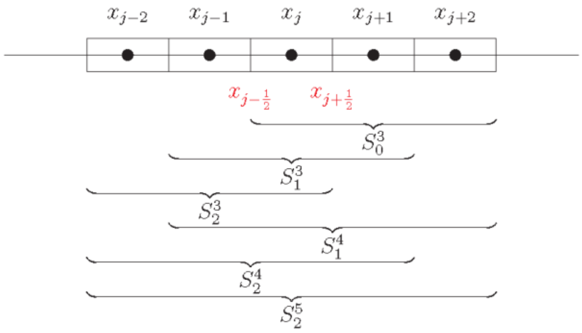

Fig. 1 All sub-stencils inside S_2^5 $(k = 3)$

$$f_{i+\frac{1}{2}} = \sum_{r=0}^{k-1} \omega_r f_{i+\frac{1}{2}}^{(k,r)}, \quad 0 \le r \le k-1 \tag{3}$$

where $f_{i+\frac{1}{2}}^{(k,r)}$ is a kth-order approximation of the flux. The flux $f_{i+\frac{1}{2}}^{(k,r)}$ satisfies (2) with $m = k$ by using the following stencil points

$$S_r^k = \{x_{i-r}, x_{i-r+1}, \cdots, x_{i-r+k-1}\} \tag{4}$$

and it is obtained by a polynomial of degree at most $k-1$, $p_r^k(x)$, which its average in $\left[x_{j-\frac{1}{2}}, x_{j+\frac{1}{2}}\right]$ equals f_j for all $x_j \in S_r^k$:

$$f_j = \frac{1}{\Delta x}\int_{x_{j+\frac{1}{2}}}^{x_{j+\frac{1}{2}}} p_r^k(\xi)d\xi, \quad x_j \in S_r^k \tag{5}$$

The coefficients ω_r are nonlinear weights which determine the contribution of each $f_{i+\frac{1}{2}}^{(k,r)}$ to $f_{i+\frac{1}{2}}$. For consistency and stability, it is required:

$$\omega_r \ge 0, \quad \sum_{r=0}^{k-1} \omega_r = 1 \tag{6}$$

In [2] after extensive numerical experiments, the following weights are proposed

$$\omega_r = \frac{\alpha_r}{\sum_{q=0}^{k-1}\alpha_q}, \quad \alpha_r = \frac{d_r}{(\beta_r + \varepsilon)^2} \tag{7}$$

where the coefficients d_r are optimal weights that generate the $(2k-1)$th-order central upwind scheme:

$$f_{i+\frac{1}{2}}^{(2k-1,k)} = \sum_{r=0}^{k-1} d_r f_{i+\frac{1}{2}}^{(k,r)} \tag{8}$$

and the parameter ε is a small number to avoid division by zero. The coefficients β_r are called the smoothness indicators and defined by

$$\beta_r = \sum_{l=1}^{k-1}\int_{x_{i-\frac{1}{2}}}^{x_{i+\frac{1}{2}}} \Delta x^{2l-1}\left(\frac{\partial^l p_r^k(x)}{\partial x^l}\right)^2 dx \tag{9}$$

It should be mentioned $\beta_r = O(h^2)$ if the function is smooth inside S_r^k and $\beta_r = O(1)$ if S_r^k contains a discontinuity.

In the literature, this method is usually represented by WENO-JS in honor of the authors of [2]. Another method is the WENO-Z scheme [16, 17] which differs from the WENO-JS scheme in the definition of α_r:

$$\alpha_r = d_r\left(1 + \left(\frac{\tau_{2k-1}}{\beta_r + \varepsilon}\right)^2\right) \tag{10}$$

$$\tau_{2k-1} = \begin{cases} |\beta_0 - \beta_{k-1}| & mod(k,2) = 1 \\ |\beta_0 - \beta_1 - \beta_{k-2} + \beta_{k-1}| & mod(k,2) = 0 \end{cases} \tag{11}$$

3- The new scheme

As described in the previous section, in a $(2k-1)$th-order WENO scheme, a linear combination of kth-order sub-stencils (S_r^k) form the $(2k-1)$th-order flux (8). These sub-stencils are inside the stencil S_{k-1}^{2k-1}. However, there are other sub-stencils inside S_{k-1}^{2k-1}, which can form the same $(2k-1)$th-order flux. For instance, Fig. 1 shows the sub-stencils inside S_2^5 $(k=3)$.

More precisely, there are $(k-s)$ sub-stencils of $(k+s)$ th-order inside S_{k-1}^{2k-1}:

$$\{S_s^{k+s}, S_{s+1}^{k+s}, \cdots, S_{k-1}^{k+s}\}, \quad 0 \le s \le k-1 \tag{12}$$

which can form

$$f_{i+\frac{1}{2}}^{(2k-1,k)} = \sum_{r=s}^{k-1} d_r^{(k+s)} f_{i+\frac{1}{2}}^{(k+s,r)} \tag{13}$$

Note that for $s=0$, (13) reduces to (8). Leaving aside the largest stencil ($s=k-1$), we have $k-1$ linear combinations to construct $f_{i+\frac{1}{2}}^{(2k-1,k)}$. For each s, we use the same procedure of the conventional WENO schemes in (7) to form a weighted linear combination of $(k+s)$th-order fluxes:

$$\tilde{f}_{i+\frac{1}{2}}^{(k+s)} = \sum_{r=s}^{k-1} \omega_r^{(k+s)} f_{i+\frac{1}{2}}^{(k+s,r)} \tag{14}$$

$$\omega_r^{(k+s)} = \frac{\alpha_r^{(k+s)}}{\sum_{q=s}^{k-1} \alpha_q^{(k+s)}}, \quad \alpha_r^{(k+s)} = \frac{d_r^{(k+s)}}{\left(\beta_r^{(k+s)} + \varepsilon\right)^2} \tag{15}$$

where the coefficients $d_r^{(k+s)}$ are optimal weights which generate the $(2k-1)$th-order central upwind scheme $f^{(2k-1,k)}$. Table 1 shows the optimal weights for $k=3$ and $k=4$ which corresponds to the fifth- and seventh-order schemes, respectively. Note that the values in rows $s=0$ are the known optimal weights of the WENO5 and WENO7 schemes. To distinguish between the flux $\tilde{f}^{(k+s)}$ in (14) and the sub-stencil fluxes $f^{(k+s,r)}$, we call the former the intermediate flux.

It is also possible to use the WENO-Z approach [17] to define $\alpha_r^{(k+s)}$:

$$\alpha_r^{(k+s)} = d_r^{(k+s)}\left(1 + \left(\frac{\tau_{2k-1}}{\beta_r^{(k+s)} + \varepsilon}\right)^2\right) \tag{16}$$

$$\tau_{2k-1} = \begin{cases} |\beta_0^{(k)} - \beta_{k-1}^{(k)}| & mod(k,2) = 1 \\ |\beta_0^{(k)} - \beta_1^{(k)} - \beta_{k-2}^{(k)} + \beta_{k-1}^{(k)}| & mod(k,2) = 0 \end{cases} \tag{17}$$

where in the definition of τ_{2k-1}, we use only the smoothness indicators of the kth-order sub-stencils.

Now, we use the intermediate fluxes (14) to construct the final flux:

$$f_{i+\frac{1}{2}} = \sum_{s=0}^{k-2} \gamma^{(k+s)} \tilde{f}_{i+\frac{1}{2}}^{(k+s)} \tag{18}$$

where $\gamma^{(k+s)}$ are the weights which to be determined. We call these weights the total weights to distinguish them from the weights $\omega_r^{(k+s)}$. Furthermore, we denote this method by WENO-C where C is the first letter of "Combined". Also, if instead of (15), the WENO-Z approach (16) is used for computing the coefficients $\alpha_r^{(k+s)}$, then we denote the new scheme by WENO-ZC.

To have proper total weights ($\gamma^{(k+s)}$) for each of the intermediate fluxes in (18), we use the same weighted linear combination as (14) to define the corresponding smoothness indicators:

$$\tilde{\beta}^{(k+s)} = \sum_{r=s}^{k-1} \omega_r^{(k+s)} \beta_r^{(k+s)} \tag{19}$$

This definition (for a fixed s) relates the smoothness indicator $\tilde{\beta}^{(k+s)}$ to the smoothness indicators of its sub-stencils. We call $\tilde{\beta}^{(k+s)}$ the total smoothness indicator of the $(k+s)$ th-order sub-stencils. Therefore, the smoothness contribution of each sub-stencil is equal to the contribution of its corresponding flux to the intermediate flux (14). This means, when comparing the stencils of two different intermediate fluxes (different s), the comparison is mostly made between the sub-stencils which have the greatest influence on that intermediate flux. In other words, if a sub-stencil flux ($f^{(k+s,r)}$) is ruled out due to intersecting a discontinuity, then its smoothness contribution is also eliminated from $\tilde{\beta}^{(k+s)}$.

Now, we define the weights $\gamma^{(k+s)}$ in a similar approach of the original WENO schemes as:

$$\gamma^{(k+s)} = \frac{\tilde{\alpha}^{(k+s)}}{\sum_{q=0}^{k-2} \tilde{\alpha}^{(k+q)}}, \quad \tilde{\alpha}^{(k+s)} = \frac{\tilde{d}^{(k+s)}}{\left(\tilde{\beta}^{(k+s)} + \varepsilon\right)^2} \tag{20}$$

where the coefficients $\tilde{d}^{(k+s)}$ determine the preference of each $\tilde{f}^{(k+s)}$ in smooth regions. Since, in smooth regions, all the intermediate fluxes in (18) reduce to the $(2k-1)$ th-order accurate flux $f^{(2k-1,k)}$, there is no preference between them. However, near discontinuities, it is desirable for small deviation of the weights from their optimal values in (14), the intermediate flux with higher-order sub-stencils is assigned a larger total weight as long as it does not spoil the ENO property of the method.

To better explain the new scheme, consider a discontinuity in cell of x_{j+1}. Therefore, except S_2^3, all the stencils in Fig. 1 contain the discontinuity. Therefore,

$$\beta_2^{(3)} = O(h^2), \quad \beta_0^{(3)}, \beta_1^{(3)} = O(1),$$
$$\beta_1^{(4)}, \beta_2^{(4)} = O(1)$$

and hence

$$\omega_2^{(3)} = O(1), \quad \omega_0^{(3)}, \omega_1^{(3)} = O(h^2),$$
$$\omega_1^{(4)}, \omega_2^{(4)} = O(1)$$

which leads to

$$\tilde{\beta}^{(3)} = O(h^2), \quad \tilde{\beta}^{(4)} = O(1)$$

and then

$$\gamma^{(3)} = O(1), \quad \gamma^{(4)} = O(h^2)$$

This means, the fourth-order intermediate flux is not considered (its contribution is very small) in construction of the final flux. This is desirable, because none of the fourth-order stencils are smooth. Now, consider a discontinuity in cell of x_{j+2}. In this case, the smooth stencils are S_1^3, S_2^3 and S_2^4. Therefore,

$$\beta_2^{(3)}, \beta_1^{(3)} = O(h^2), \quad \beta_0^{(3)} = O(1),$$
$$\beta_2^{(4)} = O(h^2), \quad \beta_1^{(4)} = O(1)$$

and

$$\omega_2^{(3)}, \omega_1^{(3)} = O(1), \quad \omega_0^{(3)} = O(h^2),$$
$$\omega_2^{(4)} = O(1), \quad \omega_1^{(4)} = O(h^2)$$

which leads to

$$\tilde{\beta}^{(3)} = O(h^2), \quad \tilde{\beta}^{(4)} = O(h^2)$$

and then

$$\gamma^{(3)} = O(1), \quad \gamma^{(4)} = O(1)$$

Table 1 Optimal weights for $k=3$ and $k=4$.

k	s	$d_0^{(k+s)}$	$d_1^{(k+s)}$	$d_2^{(k+s)}$	$d_3^{(k+s)}$
3	0	$3/10$	$6/10$	$1/10$	
3	1		$3/5$	$2/5$	
4	0	$4/35$	$18/35$	$12/35$	$1/35$
4	1		$2/7$	$4/7$	$1/7$
4	2			$4/7$	$3/7$

Table 2 L_1 error and convergence of WENO-C schemes

	Central Upwind		WENO5		WENO5-C p = 1		WENO5-C p = 2		WENO5-C p = 4	
Δx	L_1	Order	L_1	Order	L_1	Order	L_1	Order	L_1	Order
0.5^3	6.02E-04		4.17E-03		1.86E-03		1.36E-03		8.20E-04	
0.5^4	1.95E-05	4.95	1.34E-04	4.96	5.74E-05	5.02	4.22E-05	5.01	2.62E-05	4.97
0.5^5	6.18E-07	4.98	4.22E-06	4.98	1.82E-06	4.98	1.34E-06	4.98	8.29E-07	4.98
0.5^6	1.94E-08	4.99	1.33E-07	4.99	5.72E-08	4.99	4.21E-08	4.99	2.61E-08	4.99
0.5^7	6.11E-10	4.99	4.16E-09	5.00	1.79E-09	4.99	1.32E-09	4.99	8.19E-10	4.99

This means both the third- and fourth-order intermediate fluxes are present in the final flux. In this case, it is desirable the fourth-order flux has a larger total weight. This shows we require a proper choice for $\tilde{d}$ coefficients.

Through some numerical experiments, we propose

$$\tilde{d}^{(k+s)} = (1+s)^p, \quad 0 \le s \le k-2 \tag{21}$$

where p is a positive number. Therefore, it is an increasing function of s. Also, larger values of p assign larger values to the total weight of the intermediate fluxes with higher-order sub-stencils (larger s).

4- Numerical experiments

In this section, we assess the numerical performance of the new WENO scheme. We set $\varepsilon = 10^{-12}$ for WENO-JS and WENO-C and $\varepsilon = 10^{-40}$ for WENO-Z and WENO-ZC. For the time integration, the following third-order TVD Runge-Kutta scheme [29] is used

$$\begin{aligned} u^{(1)} &= u^n + \Delta t L(u^n) \\ u^{(2)} &= \frac{3}{4}u^n + \frac{1}{4}u^{(1)} + \frac{1}{4}\Delta t L\left(u^{(1)}\right) \\ u^{n+1} &= \frac{1}{3}u^n + \frac{2}{3}u^{(2)} + \frac{2}{3}\Delta t L\left(u^{(2)}\right) \end{aligned} \tag{22}$$

where Δt is the time-step.

4-1- Advection equation

The first test case is the linear advection equation:

$$u_t + u_x = 0, \quad x \in [-1,1] \tag{23}$$

First, we assess the error and convergence of the new schemes for a smooth solution. A periodic function in $[-1,1]$ is considered: $u(x,0) = \sin(\pi x)$. Since the time integration method is third-order, the time step is chosen to be $\Delta t = 0.5(\Delta x)^{\frac{5}{3}}$ in order that the error for the overall scheme is a measure of the spatial convergence only. The error of the numerical solution is computed by comparing with the exact solution at $t = 2$. Table 2 shows the L_1 norm of the error:

$$L_1 = \frac{2}{N}\sum_{i=0}^{N}\left|u_i - u_{\text{exact},i}\right|$$

For the sake of comparison, the results of the central upwind scheme (i.e. the optimal scheme) and the WENO5 scheme, are given in the table. The results show WENO5-C converges at fifth-order for different values of p. The value of the L_1 error shows WENO5-C is more accurate than WENO5. Also, increasing the value of p decreases the error and causes the error to become closer to the error of the central upwind scheme.

Table 3 compares the computational time of WENO5-C with WENO5. The compiler is the intel C++ 19.2 compiler using the Release x64 configuration on an intel 12900K CPU. The results show the computational cost of WENO5-C is only 10 percent higher than that of WENO5. This is a negligible increase in comparison to mapped WENO schemes, where the increase is about 55 precent [30, Fig. 9].

Now, we assess the performance of the scheme for a non-smooth initial condition. We use a function which contains a Gaussian-, a triangle-, a square- and a half-ellipse-wave region [2]:

Table 3 Computational time for a single time-steps in microseconds

N	WENO5	WENO5-C
201	8.6	9.7
401	17.0	19.0

$$u(x,0) = \begin{cases} \frac{1}{6}\left(Q(x,\beta,\zeta-\delta) + Q(x,\beta,\zeta+\delta) + 4(x,\beta,\zeta)\right) & x \in [-0.8,-0.6] \\ 1 & x \in [-0.4,-0.2] \\ 1 - |10(x-0.1)| & x \in [0.0,0.2] \\ \frac{1}{6}\left(R(x,\alpha,a-\delta) + R(x,\alpha,a+\delta) + 4R(x,\alpha,a)\right) & x \in [0.4,0.6] \\ 0 & otherwise \end{cases} \tag{24}$$

where

$$Q(x,\beta,\zeta) = exp(-\beta(x-\zeta)^2),$$
$$R(x,\alpha,a) = \sqrt{max(1-\alpha^2(x-a)^2, 0)}$$

and the constants are

$$a = 0.5, \quad \zeta = -0.7, \quad \delta = 0.005,$$
$$\alpha = 10, \quad \beta = ln\frac{2}{36\delta^2}$$

First, we give a description on the weights. Figure 2 shows the distribution of the weights around the discontinuity of the square wave for the WENO5-C scheme with $p = 1$. The points B and C at $x = -0.41$ and $x = -0.40$ are immediately before and after the discontinuity, respectively. At these points we have $\gamma^3 = 1$ and $\gamma^4 = 0$. This is because both the fourth-order sub-stencils (corresponding to these points) intersect the discontinuity. Therefore, the fourth-order sub-stencils are not used in the flux computation. Furthermore, the weights of the third-order sub-stencils for the point B are $(\omega_0^{(3)}, \omega_1^{(3)}, \omega_2^{(3)}) = (0,0,1)$ which means only S_2^3 is used to compute the flux (see Fig. 1). Similarly, this is the case, in the reverse order, for the point C. For the points A and D, respectively at $x = -0.42$ and $x = -0.39$, which are one point away from the discontinuity, we have $\gamma^3 = \tilde{d}^3 = \frac{1}{3}$ and $\gamma^4 = \tilde{d}^4 = \frac{2}{3}$ which means the fourth-order sub-stencils are taken into account for the flux computation. Now, we observe the weights of the fourth-order sub-stencils corresponding to the point A are $(\omega_1^{(4)}, \omega_2^{(4)}) = (0,1)$ which means only S_2^4 is used to compute the flux and S_1^4 is abandoned due to intersecting the discontinuity.

Figure 3 shows the overall distribution of the total weights γ^3 and γ^4 for the function (24). As it is observed, the total weight of the fourth-order schemes γ^4 is always lower than $\tilde{d}^4 = \frac{2}{3}$. Therefore, to increase the usage of the fourth-order schemes, it is required to increase $\tilde{d}^4$, or p in (13). As stated previously, in smooth regions, the value of the total weights are not important, because both the combination of the third- and fourth-order subs-stencils produce the fifth-order scheme. However, when the weights $\omega_r^{(3)}$ and $\omega_r^{(4)}$ deviates from their optimal values, it is desirable to use the fourth-order sub-stencils as long as it does not spoil the ENO property of the method. Therefore, in the numerical test cases, we examine several values for p.

Figure 4 shows the numerical results at $t = 8$ using $N = 201$ for the WENO5 schemes along with their combined versions, WENO5-C, and different values for the power parameter p. Also, figure 5 shows the same comparison for the WENO5-Z and WENO5-ZC schemes. Figure 4 shows the overall accuracy of the results increases by increasing p and the ENO property of the schemes are preserved. This can be observed especially near the discontinuities of the square wave and also at the foot of the Gaussian, triangle and half-ellipse waves. Furthermore, the improvements are observed at the peak of these waves. Similarly, in Fig. 5, we observe the improvement of the results for the WENO5-ZC schemes. However, since the WENO5-Z scheme is more accurate than the WENO5-JS scheme, this improvement is less than that of the WENO5-C schemes. Also, it is worth mentioning that at the peak of the half-ellipse wave, we see significant improvement for the WENO5-ZC scheme for $p = 4$.

Note that WENO schemes are nonlinear and even for a linear equation may have nonlinear behavior in different solution times. Therefore, for a deeper comparison, the error of the schemes as a function of time are given in Fig. 6 in logarithmic scale. The errors are computed at each complete time period for four intervals containing each of the four waves. Specifically, since the width of all the waves are 0.2, we consider an interval of length 0.4 centered at that wave to compute the error. We observe, for all the waves, WENO5-C has more accurate solution in comparison with WENO5. Also, it is observed using higher values for p, decreases the error.

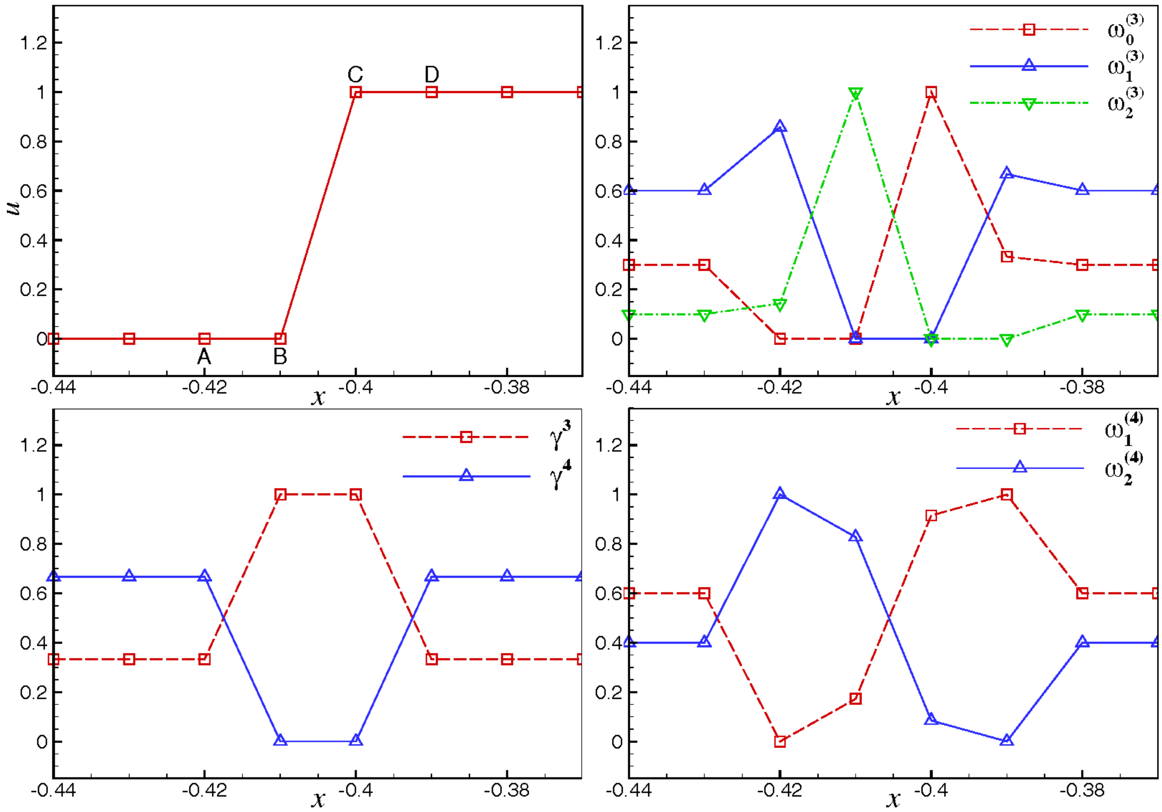

Fig. 2 The distribution of the weights near a discontinuity; top-left) the function (24), bottom-left) total weights of the third- and fourth-order stencils, top-right) weights of the third-order sub-stencils, bottom-right) weights of the fourth-order sub-stencils.

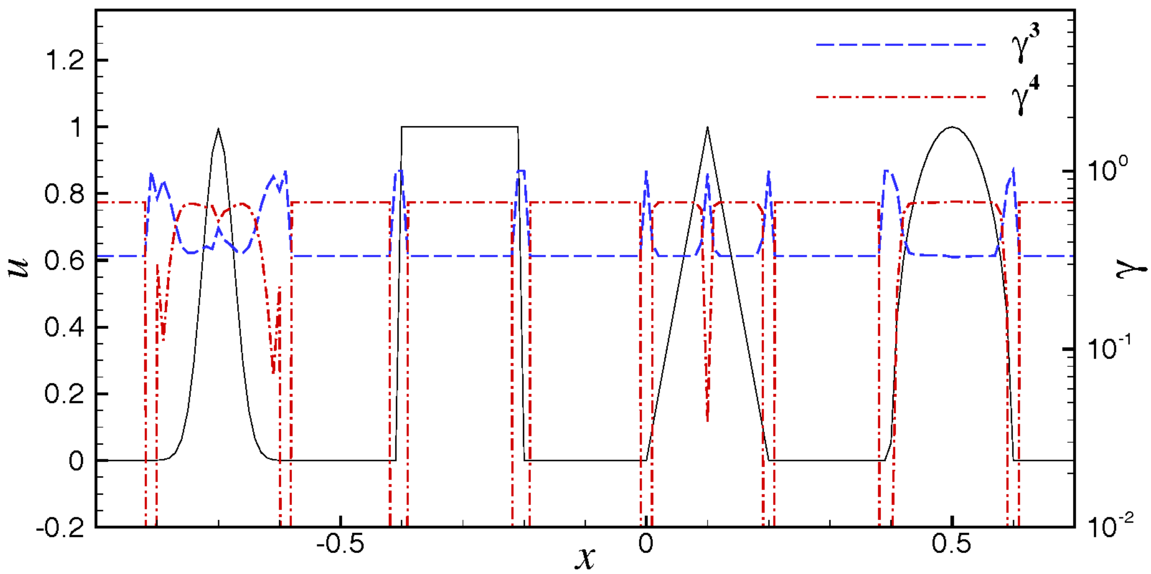

Fig. 3 The distribution of the total weights γ^3 and γ^4 for the function (24).

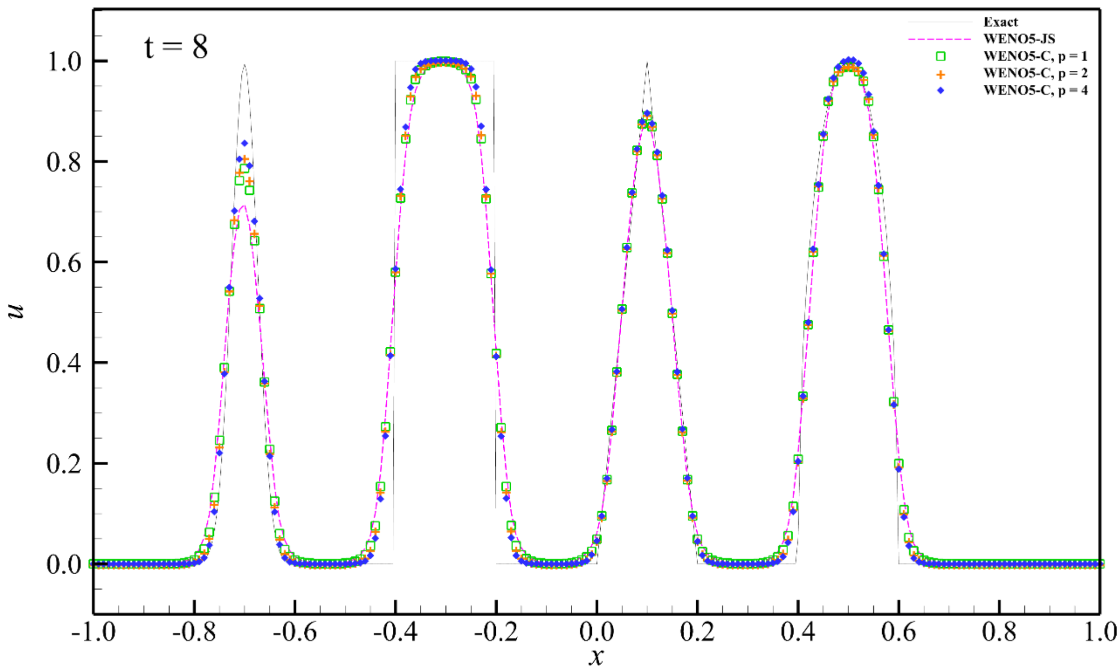

Fig. 4 Numerical solution of the advection equation by the WENO5-JS and WENO5-C schemes using $N = 201$ at $t = 8$ using different values for the power parameter p.

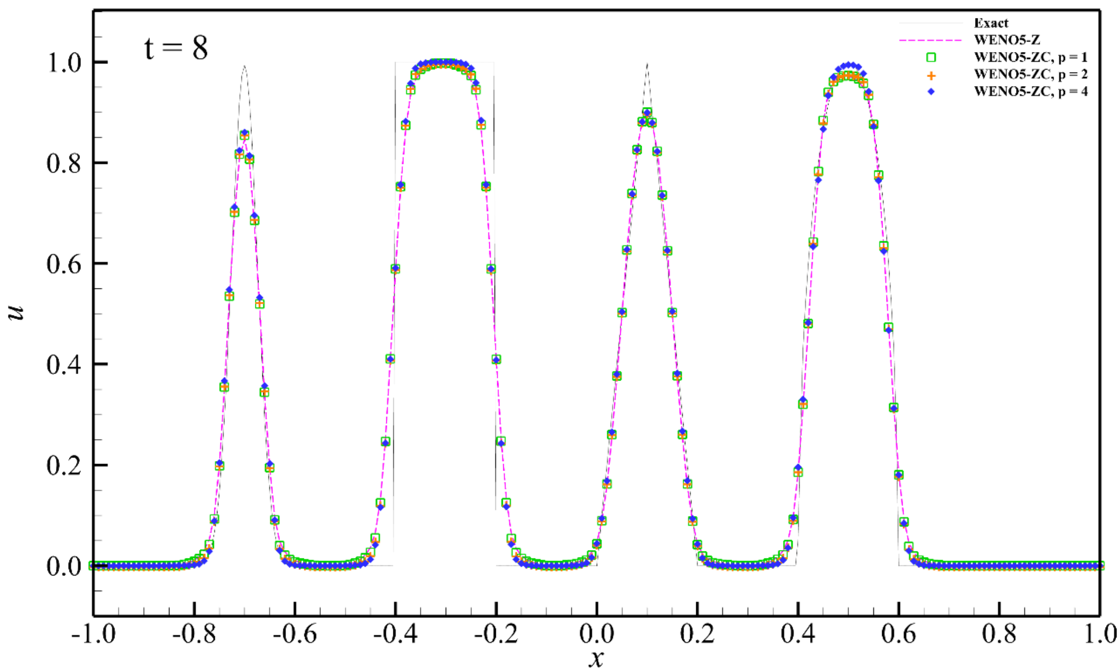

Fig. 5 Numerical solution of the advection equation by the WENO5-Z and WENO5-ZC schemes using $N = 201$ at $t = 8$ using different values for the power parameter p.

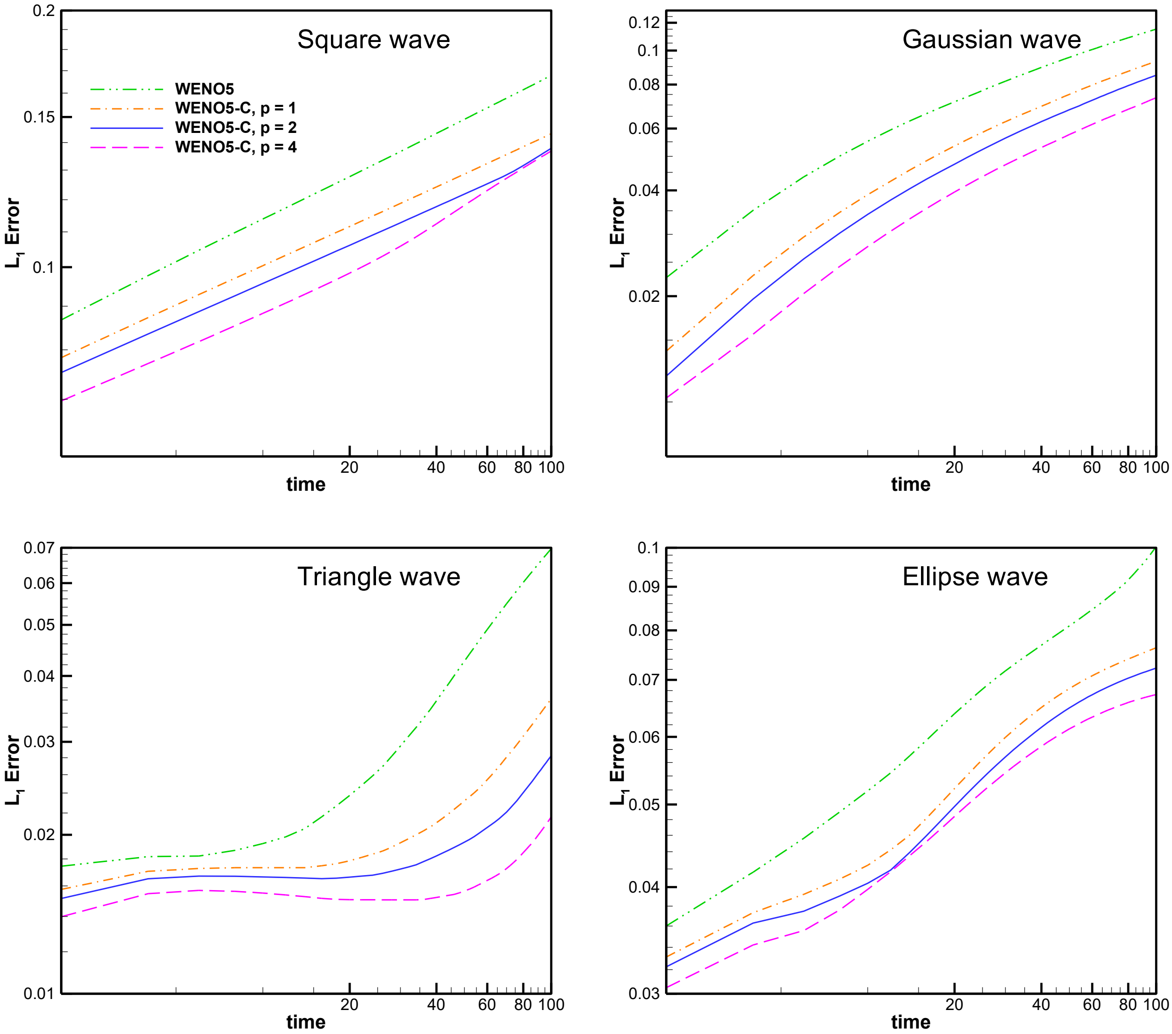

Fig. 6 L_1 error for the four waves as a function time in logarithmic scale for $N = 201$ using different values for the power parameter p.

4-2- Shock-tube problem

The second test case is the Sod shock-tube problem [31]. The governing equations are the one-dimensional Euler equations of gas dynamics:

$$U_t + F_x = 0, \quad U = \begin{pmatrix} \rho \\ \rho u \\ E \end{pmatrix}, \quad F = \begin{pmatrix} \rho u \\ \rho u^2 + p \\ (E+p)u \end{pmatrix}$$
$$E = \rho\left(e + \frac{u^2}{2}\right), \quad p = \rho e(\gamma - 1), \quad \gamma = 1.4 \tag{25}$$

where $u, \rho,\ p$ and e denote the velocity, density, pressure and internal energy per unit mass, respectively. The solution domain is [0, 10] and the left and right states of the discontinuity at $t = 0$ are

$$\begin{aligned} &(\rho_L, u_L, p_L) = (1,0,1), \quad x \leq 5 \\ &(\rho_R, u_R, p_R) = (0.125,0,0.1), \quad x > 5 \end{aligned} \tag{26}$$

where the exact solution possesses a self-similar solution which consists of a shock, a contact discontinuity and an expansion fan.

Figure 7 shows the density profile at $t = 2$ for different fifth-order schemes. The grid spacing is $\Delta x = 0.05$ (201 points) and the time marching is done using a fixed time-step of $\Delta t = 0.01$. The characteristic-wise Lax-Friedrichs flux splitting [32] is used to handle both the negative and positive wave speeds. The results show the combined schemes (WENO5-C and WENO5-ZC) have more accurate results especially around the contact discontinuity ($x \simeq 6.7$) and the left and right ends of the expansion fan. It should be mention that increasing the accuracy is achieved without appearing any spurious oscillations.

4-3- Shock-density wave interaction

This test case involves the interaction between a Mach 3 moving shock and a density wave in shape of a sine function [33]. The governing equations are the Euler equations (25). The solution domain is $[-5,\ 5]$ and the initial states of the gas are as follows

$$\begin{aligned} &(\rho_L, u_L, p_L) = (3.857143, 2.629369, 10.33333), x \leq -4 \\ &(\rho_R, u_R, p_R) = (1 + 0.2\,sin(5x), 0, 1), \qquad x > -4 \end{aligned} \tag{27}$$

Figure 8 shows the density profile at the initial time and also at $t = 1.8$. During the interaction, several shocks and high gradient regions appear. Specifically, at the time shown in the figure, the location of the moving shock is $x \approx 2.4$ and some shocks and steepening gradients are formed behind in $x \in [-2.9, 0.8]$. Also, during the interaction, the steepening gradients gradually form shocks. At the time $t = 1.8$, two of these steepening gradients at $x \approx -2.6$ and $x \approx -1.6$, already become discontinuous.

In this test case, we consider the seventh-order scheme. Figure 9 shows the density distribution using $N = 201$ points ($\Delta x = 0.05$) at $t = 1.8$. Also, the time-step is $\Delta t = 0.002$. Comparing the results, especially in the high-gradient region, shows that WENO7-C and WENO7-ZC give considerably more accurate results than WENO7-JS and WENO7-Z, respectively. Furthermore, we observe the results of WENO7-ZC are more accurate than those of WENO7-C.

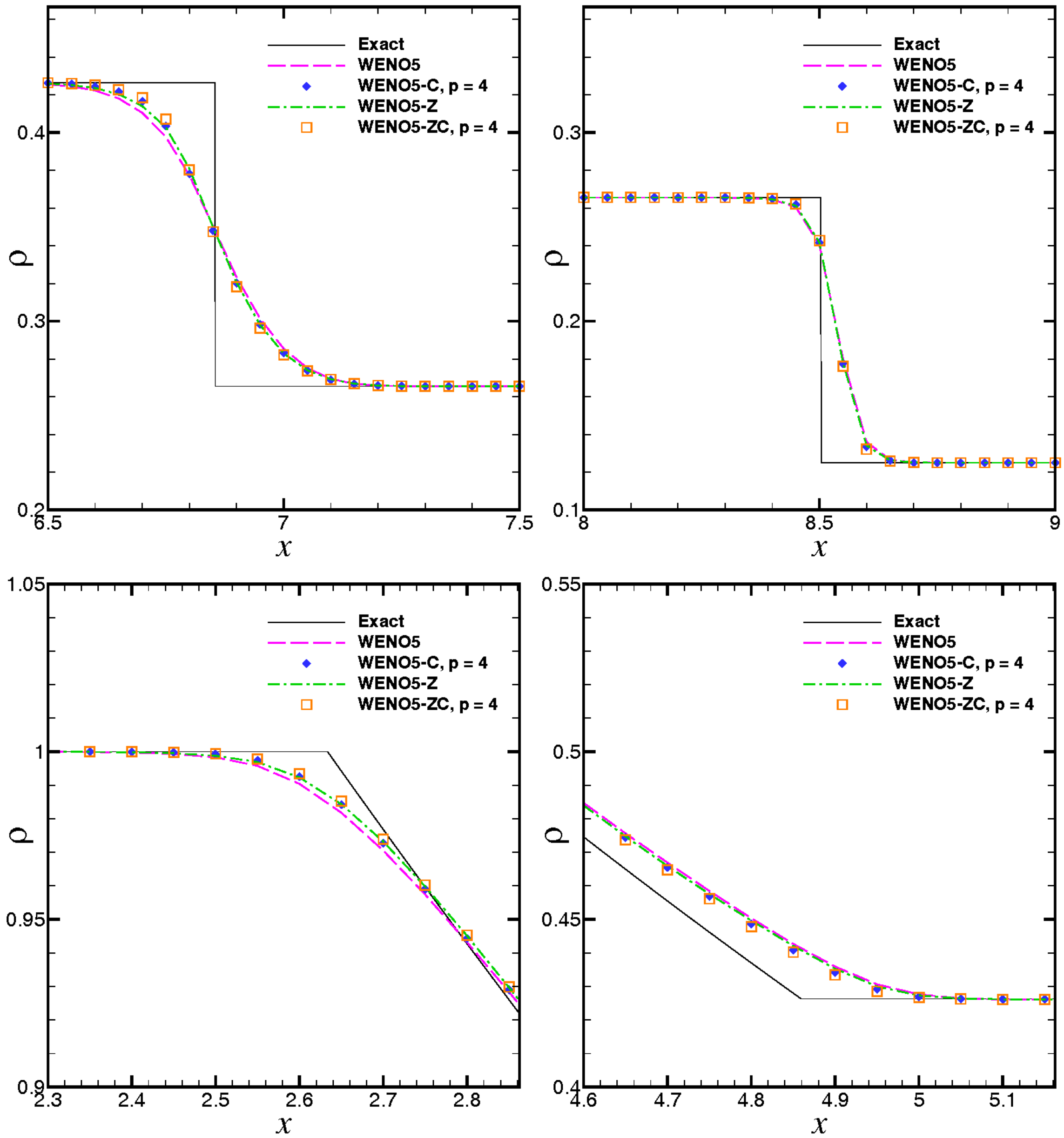

Fig. 7 The density profile of the Sod shock-tube problem around the contact discontinuity (top-left), the shock (top-right) and the left and right ends of the expansion fan (bottom) using $N = 201$ at $t = 2$.

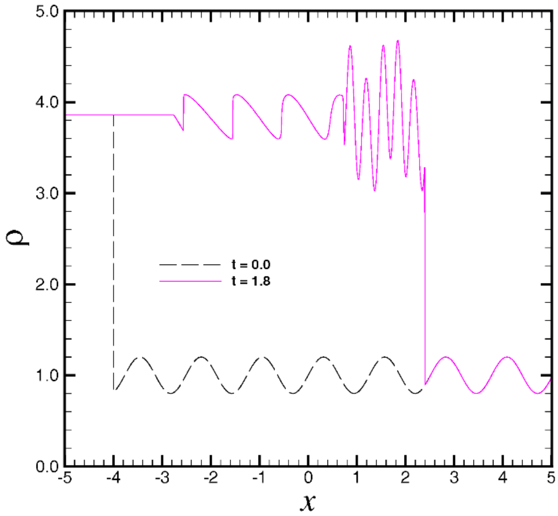

Fig. 8 The density profile of the shock-density wave interaction problem at $t = 0$ and $t = 1.8$.

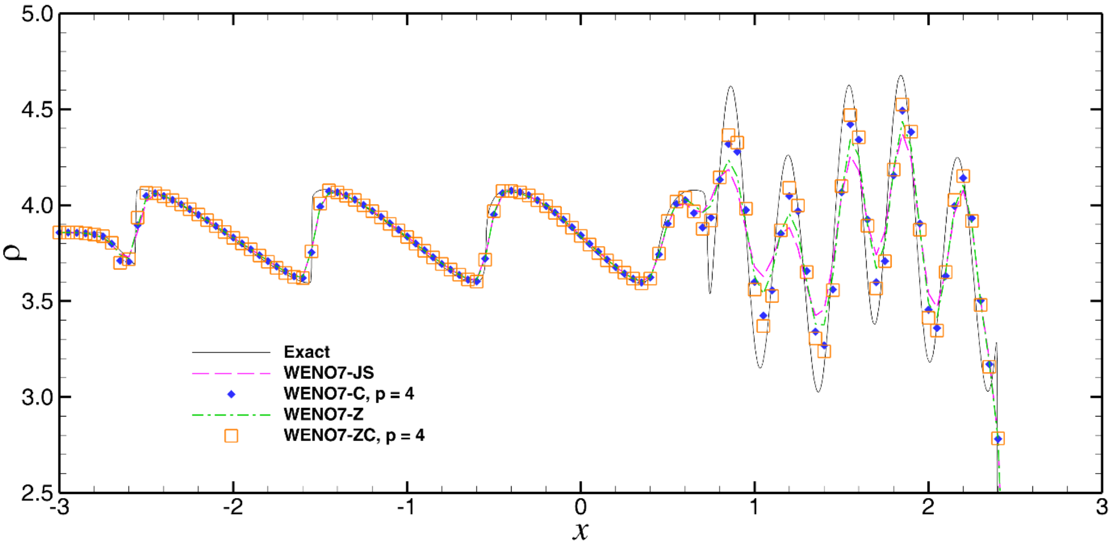

Fig. 9 The density profile of the shock-density wave interaction problem using $N = 201$ at $t = 1.8$ for the seventh-order WENO schemes.

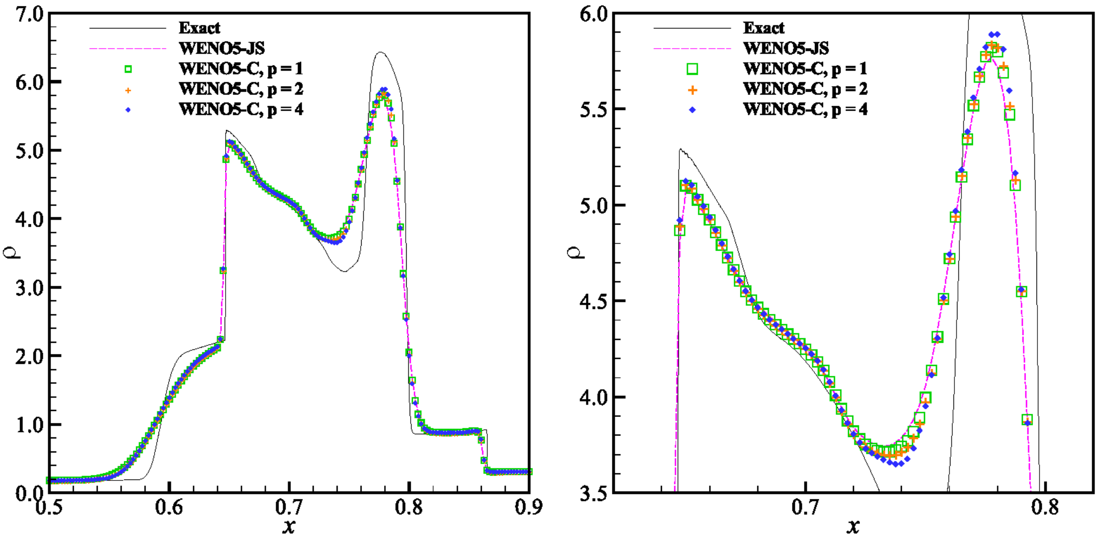

Fig. 10 The density profile of the interacting blast waves problem using $N = 401$ at $t = 0.038$ for the fifth-order WENO schemes.

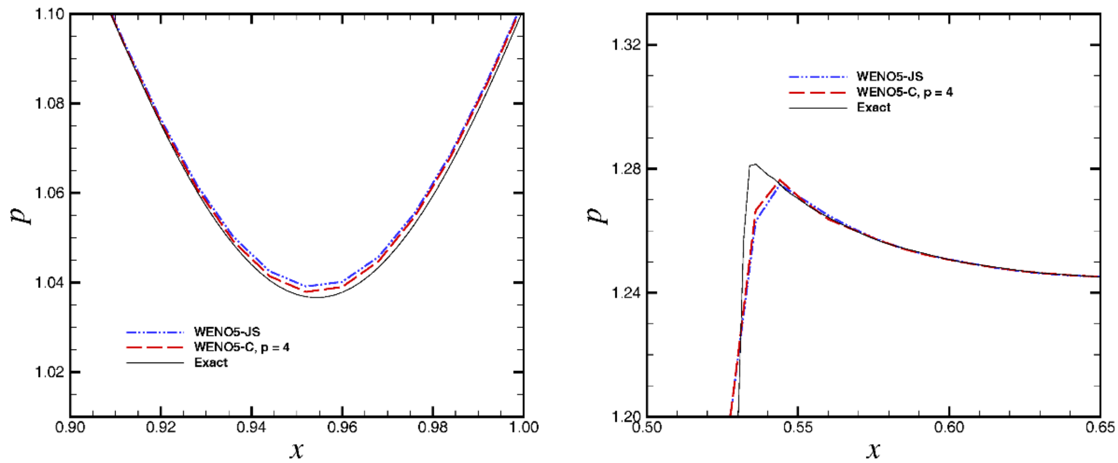

Fig. 11 The pressure profile of the shock-vortex interaction problem along $y = 0.5$ section at $t = 0.6$

4-4- Interacting blast waves

This is a very difficult test case for shock capturing schemes [34]. It involves several interactions between strong shocks, rarefaction waves and contact discontinuities. The solution domain is $[0,\ 1]$ and the initial condition consists of three constant states where the pressure in the middle part is significantly smaller than those in the left and right parts:

$$(\rho, u, p) = \begin{cases} (1,0,1000) & 0.0 \le x < 0.1 \\ (1,0,0.01) & 0.1 \le x < 0.9 \\ (1,0,100) & 0.9 \le x \le 1.0 \end{cases} \quad (28)$$

The low pressure of the middle part, in case of appearing oscillations around the shocks, can cause negative pressure and therefore the simulation failure.

Figure 10 compares the results of the fifth-order schemes at $t = 0.038$. The results are presented for 401 grid points and 800 time-steps with $\Delta t = 4.75 \times 10^{-5}$. The results show that the WENO5-C schemes are more accurate than the WENO5-JS scheme especially at the peak and valley ($x \approx 0.74$ and $x \approx 0.78$ in the zoomed view). Also, close examination reveals a slightly sharper shock (at $x \approx 0.64$) is obtained using the WENO5-C scheme. Again, it is observed that the accuracy of the results increases and the ENO property of the method is preserved.

4-5- Shock-vortex interaction

This is a two-dimensional test case where a vortex passes through a stationary normal shock [2]. The governing equations are the two-dimensional Euler equations:

$$U_t + F_x + G_y = 0,$$
$$U = \begin{pmatrix} \rho \\ \rho u \\ \rho v \\ E \end{pmatrix}, \quad F = \begin{pmatrix} \rho u \\ \rho u^2 + \rho \\ \rho uv \\ (E+\rho)u \end{pmatrix}, \quad G = \begin{pmatrix} \rho v \\ \rho vu \\ \rho v^2 + p \\ (E+p)v \end{pmatrix} \quad (29)$$
$$E = \rho\left(e + \frac{u^2+v^2}{2}\right), \quad p = \rho e(\gamma - 1), \quad \gamma = 1.4$$

The problem domain is $[0,2] \times [0,1]$ and the vertical shock is stationary and located at $x = 0.5$. The shock Mach number is 1.1. The left state of the shock is

$$(\rho_L, u_L, v_L, p_L) = \left(1, 1.1\sqrt{\gamma}, 0, 1\right)$$

and the right state is obtained using the normal-shock relations. A small isentropic vortex is superposed to the shock left state. The vortex center is at $(x_c, y_c) = (0.25, 0.5)$ and its properties (denoted by δ) is added to the velocity (u, v), temperature ($T = \frac{p}{\rho}$), and entropy ($s = ln(\frac{p}{\rho^\gamma})$) of the shock left state:

$$(\delta_u, \delta_v) = \kappa\eta e^{\alpha(1-\eta^2)}(\sin\theta, -\cos\theta),$$
$$\delta T = -\frac{(\gamma-1)\kappa^2 e^{2\alpha(1-\eta^2)}}{4\alpha\gamma}, \quad \delta s = 0$$

where $\kappa = 0.3$ is the vortex strength and $\eta = \frac{r}{r_c}$, where r and θ are the polar coordinates with respect to the vortex center. Also, $r_c = 0.05$ is the vortex critical radius and $\alpha = 0.204$ is the vortex decay rate.

Figures 11 displays the pressure distribution along the $y = 0.5$ section at $t = 0.6$ where the vortex has passed the shock. The results obtained by WENO5-JS and WENO5-C are compared after the shock and also at the vortex core. In both regions, we observe more accurate results are obtained by the WENO5-C scheme.

5- Conclusions

We introduced a new method to improve the accuracy of the WENO schemes, which we called WENO-C. The "C" stands for combined. The goal was to use all the available sub-stencils of different orders, from kth- to $(2k-2)$th-order, to construct the flux. First, $(k-1)$ intermediate fluxes were constructed using a weighted combination of the sub-stencils of the same order of accuracy, similar to the conventional WENO schemes. Then, the intermediate fluxes were combined to form the final flux. The key idea was to define suitable weights (called total weights) for the linear combination of these intermediate fluxes. This was done by defining the total weights as a function of their corresponding total smoothness indicator and a coefficient to control the contribution of each intermediate flux to the final flux. The total smoothness indicator of each intermediate flux was defined as a weighted combination of the smoothness indicators of its sub-stencils where each weight was the same as its corresponding flux weight in the construction of that intermediate flux. The numerical results showed that this way of defining the total smoothness indicators properly allows to use all the sub-stencils which does not intersect the discontinuity.

Furthermore, by using a simple power function, suitable coefficients for the total weights were obtained. With the power parameter p in the range from 2 to 4, we were able to increase the effect of higher-order sub-stencils and therefore increase the results accuracy. Numerical experiments showed that the new method while increased the overall accuracy of the results, was resistant against spurious oscillations near discontinuities and therefore suitably preserved the ENO property.

Acknowledgments

The authors would like to thank the University of Tehran for financial support for this research under grant number 04/1/28745.

Ethics Approval

The scientific content of this article is the result of the authors' research and has not been published in any Iranian or international journal.

Conflict of Interest

There is no conflict of interest to declare.

References

[1] X. D. Liu, S. Osher, and T. Chan, "Weighted essentially non-oscillatory schemes," J. Comput. Phys., vol. 115, pp. 200–212, 1994.
doi: http://doi.org/10.1006/jcph.1994.1187

[2] G. S. Jiang and C. W. Shu, "Efficient implementation of weighted ENO schemes," J. Comput. Phys., vol. 126, pp. 202–228, 1996.
doi: http://doi.org/10.1006/jcph.1996.0130

[3] R. Bozorgpoor, M. Shafaee, and H. M. Darian, "Simulation of shock-containing flows using a compact finite difference scheme and a weighted essentially non-oscillatory filter," Modares Mech. Eng., vol. 17, no. 5, pp. 201–210, 2017.
doi: doi.org/20.1001.1.10275940.1396.17.5.48.6

[4] Y. Shekari and A. Tayebi, "Numerical simulation of two-phase flows using drift flux model and DG-ADER scheme," Modares Mech. Eng., vol. 15, no. 9, pp. 51–58, 2015.
doi: doi.org/20.1001.1.10275940.1394.15.9.14.6

[5] A. K. Henrick, T. D. Aslam, and J. M. Powers, "Mapped weighted essentially non-oscillatory schemes: Achieving optimal order near critical points," J. Comput. Phys., vol. 207, no. 2, pp. 542–567, 2005.
doi: http://doi.org/10.1016/j.jcp.2005.01.023

[6] H. Feng, F. Hu, and R. Wang, "A new mapped weighted essentially non-oscillatory scheme," J. Sci. Comput., vol. 51, no. 2, pp. 449–473, 2012.
doi: http://doi.org/10.1007/s10915-011-9554-7

[7] H. Feng, C. Huang, and R. Wang, "An improved mapped weighted essentially non-oscillatory scheme," Appl. Math. Comput., vol. 232, pp. 453–468, 2014.
doi: http://doi.org/10.1016/j.amc.2013.12.064

[8] R. Wang, H. Feng, and C. Huang, "A new mapped weighted essentially non-oscillatory method using rational mapping function," J. Sci. Comput., vol. 67, no. 2, pp. 540–580, 2016.
doi: http://doi.org/10.1007/s10915-015-0094-4
[9] U. S. Vevek, B. Zang, and T. H. New, "Adaptive mapping for high order WENO methods," J. Comput. Phys., vol. 381, pp. 162–188, 2019.
doi: http://doi.org/10.1016/j.jcp.2019.01.006
[10] U. S. Vevek, B. Zang, and T. H. New, "A new mapped WENO method for hyperbolic problems," Aerospace, vol. 9, no. 7, Art. no. 351, 2022.
doi: http://doi.org/10.3390/aerospace9070351
[11] Z. Hong, Z. Ye, and X. Meng, "A mapping-function-free WENO-M scheme with low computational cost," J. Comput. Phys., vol. 405, Art. no. 109145, 2020.
doi: http://doi.org/10.1016/j.jcp.2019.109145
[12] F. Hu, "High-order mapped WENO methods with improved efficiency," Comput. Fluids, vol. 219, Art. no. 104874, 2021.
doi: http://doi.org/10.1016/j.compfluid.2021.104874
[13] X. Zhang, C. Yan, and F. Qu, "An efficient smoothness indicator mapped WENO scheme for hyperbolic conservation laws," Comput. Fluids, vol. 240, Art. no. 105421, 2022.
doi: http://doi.org/10.1016/j.compfluid.2022.105421
[14] S. Tang and M. Li, "A novel high efficiency adaptive mapped WENO scheme," Comput. Math. Appl., vol. 124, pp. 149–162, 2022.
doi: http://doi.org/10.1016/j.camwa.2022.07.005
[15] R. Li and W. Zhong, "A robust and efficient component-wise WENO scheme for Euler equations," Appl. Math. Comput., vol. 438, Art. no. 127583, 2023.
doi: http://doi.org/10.1016/j.amc.2022.127583
[16] R. Borges, M. Carmona, B. Costa, and W. S. Don, "An improved weighted essentially non-oscillatory scheme for hyperbolic conservation laws," J. Comput. Phys., vol. 227, no. 6, pp. 3191–3211, 2008.
doi: http://doi.org/10.1016/j.jcp.2007.11.038
[17] M. Castro, B. Costa, and W. S. Don, "High order weighted essentially non-oscillatory WENO-Z schemes for hyperbolic conservation laws," J. Comput. Phys., vol. 230, no. 5, pp. 1766–1792, 2011.
doi: http://doi.org/10.1016/j.jcp.2010.12.012
[18] Y. Wang, B.-S. Wang, and W. S. Don, "Generalized sensitivity parameter free fifth order WENO finite difference scheme with Z-type weights," J. Sci. Comput., vol. 81, no. 3, pp. 1329–1358, 2019.
doi: http://doi.org/10.1007/s10915-019-01040-y
[19] S. Rathan, N. R. Gande, and A. A. Bhise, "Simple smoothness indicator WENO-Z scheme for hyperbolic conservation laws," Appl. Numer. Math., vol. 157, pp. 255–275, 2020.
doi: http://doi.org/10.1016/j.apnum.2020.05.010
[20] X. Luo and S.-P. Wu, "An improved WENO-Z+ scheme for solving hyperbolic conservation laws," J. Comput. Phys., vol. 445, Art. no. 110608, 2021.
doi: http://doi.org/10.1016/j.jcp.2021.110608
[21] A. Kumar, B. Kaur, and R. Kumar, "A new fifth order finite difference WENO scheme to improve convergence rate at critical points," Wave Motion, vol. 109, Art. no. 102859, 2022.
doi: http://doi.org/10.1016/j.wavemoti.2021.102859
[22] S. Tang and M. Li, "High-resolution mapping type WENO-Z schemes for solving compressible flow," Int. J. Numer. Methods Fluids, vol. 96, no. 6, pp. 1031–1056, 2024.
doi: http://doi.org/10.1002/fld.5261
[23] S. Amat, J. Ruiz, and C.-W. Shu, "On new strategies to control the accuracy of WENO algorithms close to discontinuities," SIAM J. Numer. Anal., vol. 57, no. 3, pp. 1205–1237, 2019.
doi: http://doi.org/10.1137/18M1203534
[24] S. Amat, J. Ruiz, and C.-W. Shu, "On a new WENO algorithm of order 2r with improved accuracy close to discontinuities," Appl. Math. Lett., vol. 105, Art. no. 106335, 2020.
doi: http://doi.org/10.1016/j.aml.2020.106335
[25] S. Amat, J. Ruiz, and C.-W. Shu, "On new strategies to control the accuracy of WENO algorithm close to discontinuities II: Cell averages and multiresolution," J. Comput. Math., vol. 38, no. 4, pp. 661–682, 2020.
doi: http://doi.org/10.4208/jcm.1912-m2019-0099
[26] S. Amat, J. Ruiz-Álvarez, C.-W. Shu, and D. F. Yáñez, "Cell-average WENO with progressive order of accuracy close to discontinuities with applications to signal processing," Appl. Math. Comput., vol. 403, Art. no. 126248, 2021.
doi: http://doi.org/10.1016/j.amc.2021.126248
[27] S. Amat, J. Ruiz-Álvarez, C.-W. Shu, and D. F. Yáñez, "On the approximation of derivative values using a WENO algorithm with progressive order of accuracy close to discontinuities," Comput. Appl. Math., vol. 41, no. 6, Art. no. 249, 2022.
doi: http://doi.org/10.1007/s40314-022-01911-5
[28] S. Amat, A. Baeza, J. Ruiz, and C.-W. Shu, "On a new centered strategy to control the accuracy of weighted essentially non oscillatory algorithm for conservation laws close to discontinuities," Numer. Methods Partial Differ. Equ., vol. 37, no. 1, pp. 172–195, 2021.
doi: http://doi.org/10.1002/num.22617
[29] C. W. Shu and S. Osher, "Efficient implementation of essentially non-oscillatory shock-capturing schemes," J. Comput. Phys., vol. 77, no. 2, pp. 439–471, 1988.
doi: http://doi.org/10.1016/0021-9991(88)90177-5
[30] H. M. Darian, "Comparison of weighted essentially non-oscillatory schemes for long time marching of the wave equation," Amirkabir J. Mech. Eng., vol. 56, no. 8, pp. 1159–1182, 2024.
doi: http://doi.org/10.22060/mej.2025.23450.7763
[31] G. A. Sod, "A survey of several finite difference methods for systems of nonlinear hyperbolic conservation laws," J. Comput. Phys., vol. 27, no. 1, pp. 1–31, 1978.
doi: http://doi.org/10.1016/0021-9991(78)90023-2
[32] C. W. Shu, "Essentially non-oscillatory and weighted essentially non-oscillatory schemes for hyperbolic conservation laws," NASA/CR-97-206253, ICASE Rep. 97-65, 1997.
[33] C. W. Shu and S. Osher, "Efficient implementation of essentially non-oscillatory shock-capturing schemes, II," J. Comput. Phys., vol. 83, no. 1, pp. 32–78, 1989.

doi: http://doi.org/10.1016/0021-9991(89)90222-2
[34] P. R. Woodward and P. Colella, "The numerical simulation of two-dimensional fluid flow with strong shocks," J. Comput. Phys., vol. 54, no. 1, pp. 115–173, 1984.
doi: http://doi.org/10.1016/0021-9991(84)90142-6